Creep, stick-slip, and dry-friction dynamics: Experiments and a heuristic model

F. Heslot, T. Baumberger, and B. Perrin
Laboratoire de Physique de la Matière Condensée de l'Ecole Normale Supérieure, 24 rue Lhomond, 75231 Paris Cedex 05, France

B. Caroli* and C. Caroli
Groupe de Physique des Solides, Université Paris VII, 2 place Jussieu, 75251 Paris Cedex 05, France
(Received 7 October 1993)

We perform an extensive study of the dry-friction dynamics of a paper-on-paper system. We explore the dynamical phase diagram by systematically varying the relevant control parameters (driving velocity V, slider mass M, and loading machine stiffness k). A set of experimental results gives strong proof that the low-velocity dynamics is controlled by a creep process, in agreement with previous results from rock mechanics and metals [C. H. Scholz, *The Mechanics of Earthquakes and Faulting* (Cambridge University Press, Cambridge, 1990), Chap. 2 and references therein; E. Rabinowicz, Proc. Phys. Soc. 71, 668 (1958) and references therein]. At higher velocities, a crossover to inertial dynamics is observed. In each regime, when k is increased, the system bifurcates from periodic stick-slip to steady sliding: in the creep regime, the bifucation is a direct Hopf one; in the inertial regime it becomes subcritical. We identify, from comparison of the time dependence of the static friction coefficient $\mu_s(t)$ and of the velocity dependence of the stationary dynamic one, $\mu_d(V)$, a memory length of the order of 1 μm. The V dependence of $\mu_d(V)$ changes from V weakening to V strengthening at the creep-inertial crossover. We propose a heuristic model of low-velocity friction based on two main ingredients: (i) following and extending the ideas of Ruina [J. Geophys. Res. **88**, 10 359 (1983)], we define a phenomenological contact age accounting for the renewal of physical contacts on the scale of the memory length, and (ii) we assume that the dynamics is controlled by the Brownian motion of an effective creeping volume in a pinning potential, the strength of which increases with age. The crossover from creep to inertial motion then naturally appears as the runaway threshold between thermally activated and free motion. The bifurcation analysis in the creep regime is compared in detail with experimental results, yielding a very satisfactory agreement. When confronted with rock mechanics results, this study strongly suggests that low-velocity creep is quite generic; further studies of this process should in particular bear on models of earthquake dynamics.

PACS number(s): 05.45.+b, 46.30.Pa, 62.20.Hg, 91.30.Px

I. INTRODUCTION

Basic studies of the physics of dry friction were pursued quite actively up till the mid sixties. A semi-phenomenological theory was then expounded in the landmark books of Bowden and Tabor [1] and of Rabinowicz [2]. It has remained up to now the standard frame of work in the field, with the noticeable exception of recent contributions from the rock mechanics community [3].

The interest of physicists for solid friction has recently been revived by both the following:

(i) The progress of lubrication studies on the microscopic scale [4,5], the control and accuracy of which has improved spectacularly in the past few years, opening the way to microscopic modeling [6].

(ii) The blooming of earthquake models, which, follow-

ing Carlson and Langer [7], suggests that seismic dynamics might be primarily due to deterministic nonlinear effects.

The self-critical features of the dynamics emerging from this class of models are intimately related to the specificities of the constitutive law relating the local friction force to the local slip velocity. Most authors assume for this forms that rely on what we will call the standard model of solid-on-solid friction. This can be, for our present purpose, schematically summarized as follows:

(a) The friction force is due to the shear strength of the "junctions," i.e., areas of real atomic or molecular contact between the two solids. These are randomly distributed in space over the area of apparent contact, and their lateral dimensions lie typically in the 1–10-μm range. This force is expressed as [1,2]

$$F = s A_{\text{real}} , \qquad (1)$$

with s a typical junction shear strength. A_{real} is the total area of real contact, which in turn is related to the normal load Mg (with M the "mass of the slider") by

$$Mg = p_m A_{\text{real}} , \qquad (2)$$

*Also at Département de Physique, Faculté des Sciences, Université de Picardie, 33 rue Saint-Leu, 80039, Amiens Cedex, France.

with p_m the flow pressure of the softer material close to the contacts. This picture, elaborated by Bowden and Tabor, accounts for Amontons's law, which states that the friction force is independent of the apparent area of contact. It relies on a model in which the junctions— whether of the "weld" or of the "indentation" type— increase their area by plastic flow until the stress they sustain reduces to the yield one.

(b) When starting from rest, sliding motion starts only once a finite shearing force F_s (parallel to the plane of contact) is reached. This defines the static normalized threshold $\mu_s = F_s/Mg$.

(c) The general accepted wisdom then states that, once sliding has started, the friction force drops to its kinetic value $\mu_d(V) < \mu_s$. This quantity is, in principle, though this is not always explicitly stated, the force measured when friction takes place at the *constant* velocity V. This immediately leads to a nontrivial problem. Indeed, as is the case in all mechanical studies, the stiffness of the loading machine plays a crucial part in the dynamics of the frictional motion. As is well known from everyone's experience of squeaking noises, when pulled at a constant driving velocity, solids very often do not move steadily, but by an alternation of slides and periods of rest, called stick-slip (SS). SS can be observed whatever the chemical nature of the solids in contacts and the state of their surfaces, provided that the loading system is soft enough, while steady sliding is obtained with stiff machines and/or high velocities. A friction experiment setup (solids in sliding contact plus driving machine) can obviously be viewed as a dynamical system subject to the stick-slip instability. It is therefore natural to try and characterize its behavior in terms of a "dynamical phase diagram" in the space of the control parameters (pulling velocity V, spring constant k measuring the stiffness of the loading system, and mass M), as was attempted in some of the early experiments of Rabinowicz [2]. Such a study was recently performed by Gu and Wong [8] on rock-gouge systems.

More systematic dynamical studies on various materials are clearly needed in order to unravel the respective roles and ranges of relevance of friction and inertia. This is necessary to understand in more detail the intrinsic characteristics of friction dynamics which are, in particular, the keystone of deterministic earthquake models.

The crucial physical ingredient responsible for their complex behavior is the "velocity-weakening" phenomenon: one interpolates between the static threshold μ_s and a smaller kinetic value μ_d, which may or may not be velocity dependent, by defining a region of decreasing friction coefficient. This, tacitly, implies that the $\mu_d(V)$ behavior, measured in steady-state regime, remains valid for unsteady motion, V being, now, taken to be the *instantaneous* velocity $\dot{x}$ of the slider.

The validity of this picture is quite unclear, as far as velocity weakening, which entails linear instability of steady sliding, seems incompatible with the experimental wisdom, stating that it is always possible to stabilize against SS by using a stiff enough loading. In such a situation, how should an unambiguous value of μ_d be measured? Is it legitimate to extend $\mu_d(V)$ into $\mu_d(\dot{x})$? If so,

is this true on all length scales? Such questions have already been raised by several authors [3,9–11], who suggest that the kinetic friction force depends not only on the instantaneous velocity but on the previous dynamical history of the solid-solid contact(s), usually referred to as the "memory effect."

Following, and confirming, the pioneering experiments of Rabinowicz [12] on metals, studies of rock friction indeed provide evidence that:

(i) The static threshold μ_s increases slowly with the duration of stationary contact prior to pulling. Different phenomenological expressions of $\mu_s(t)$ have been suggested to fit the data [9], among which is a dependence of the form [3]

$$\mu_s(t) = a_s + b_s \ln(t) . \tag{3}$$

(ii) At low pulling velocities (typically $V \lesssim 1$ μm/s), there is evidence of slow relaxation under load [13]. It is no longer possible to speak of a truly motionless "stick state," but, rather, of stress-induced creep, which suggests a continuous crossover between stick and slip.

(iii) Rabinowicz has accumulated several pieces of semiquantitative evidence for the existence of a memory effect characterized by a *length* [12].

(iv) Experiments on rock friction [3,14,15] have led to the same kind of conclusions: indentation experiments provide direct evidence of a slow relaxation under static load, compatible with a logarithmic law. This relaxation is faster in chemical environments known to promote rock plasticity. Measured $\mu_s(t)$ are compatible with expression (3). A velocity-weakening regime with steady sliding is observed, with a linear dependence of μ_d on $\ln V$.

Moreover, comparison of $\mu_s(t)$ and $\mu_d(V)$, although measured on different kinds of rocks, suggests [16] that it might be possible to define a material and structure-dependent length such that

$$\mu_d(V) = \mu_s(D_0/V) , \tag{4}$$

with D_0 typically in the range of micrometers. Analysis of the dynamical response to velocity jumps also led Dieterich [14] to conclude to the existence of a characteristic velocity-independent relaxation length, of the same order of magnitude, in the velocity-weakening regime.

This set of experimental results led Ruina [10] to propose a model that introduces the idea that solid-solid contacts obey a slow dynamics described by a phenomenological constitutive state variable. The law describing the time evolution of this variable is chosen so as to be compatible both with the existence of a memory length and with the observed $\ln V$-weakening dependence of $\mu_d(V)$. Such a model leads to a retarded frictional dynamics and, so, precludes the identification between $\mu_d(V)$ and $\mu_d(\dot{x})$ in the steady regime. Stability analysis then leads [10,11] to predict that, in the k-V plane, SS and steady sliding should occur, respectively, below and above a Hopf bifurcation curve of the form

$$k_c = k_{c0} + CV^2 , \tag{5}$$

where C is a positive constant.

This model, although opening onto a very promising wealth of dynamical behaviors [17], still suffers from two main drawbacks. First, expression (5) predicts that, for $k < k_{c0}$, SS should prevail at all pulling velocities, while, for $k > k_{c0}$, it should occur in the large-V limit, contrary to usual experimental evidence. Second, the evolution equation for the state variable ϕ entails that this quantity is constant for a motionless contact. So, the model cannot account for a time dependence of μ_s.

More recently, Gu and Wong [8] were able to account for their experimental results by resorting to a more complicated version of Ruina's model, with two state variables, and in which they impose a high-velocity cutoff on the friction law. In this situation, and in view of the quite surprising similarity of the low-velocity frictional behavior of rock-rock and metal-metal systems, we have undertaken, in the spirit of nonlinear dynamics studies, a systematic investigation of the low-velocity frictional dynamics within a wide range of stiffness. We have chosen to work with Bristol board rubbing on Bristol board. This system was finally selected for its highly periodic and reproducible behavior in the SS regime. This is to be related with its good surface homogeneity and resistance to wear. We have varied V from 10^{-2} to 5×10^4 μm s^{-1}, k from 10^2 to 10^6 N m^{-1}, M from 0.3 to 3 kg.

We have found it necessary to distinguish between a low-velocity and a high-velocity regime:

(i) The low-velocity dynamics is primarily governed by slow contact relaxation and creep phenomena. In this regime, the steady $\mu_d(V)$ decreases logarithmically with V and Eq. (3) holds with a memory length $D_0 \approx 1$ μm. Extensive exploration of the k-V space shows that the SS and steady regimes are separated by a bifurcation of the Hopf type.

(ii) The dynamical system crosses over, at large V's, from this creep-dominated regime to an inertia-dominated regime. This crossover occurs when the inertial and creep characteristic times $(M/k)^{1/2}$ and D_0/V are comparable. In the inertial regime, the steady $\mu_d(V)$ increases with V and the SS–steady sliding bifurcation becomes discontinuous (subcritical) and noise sensitive.

This set of experimental results leads us to propose a simple heuristic model, inspired by the ideas of Rabinowicz as extended by the rock mechanicians [3]. This model provides a coherent frame of interpretation of all the observations. It relies on two main physical ingredients. First, the low-velocity rubbing motion is described as a thermally activated creep process in a pinning potential. Second, the corresponding pinning strength is assumed to increase with the "age" of contacts. We extend Ruina's description of the slow age dynamics [10] so as to bridge between rest and motion.

We are thus able to account for the low-velocity stability diagram. The crossover to inertial behavior is interpreted in this model as the runaway threshold due to stress-induced depinning. The model also accounts qualitatively for the crossover from decreasing to increasing $\mu_d(V)$.

This leads us to confirm the previous suggestions that low-velocity friction is strongly influenced by the slow, plastic, evolution of the surfaces in contact. Accordingly,

it obeys in this regime a more complex dynamics than that assumed by the standard description, a conclusion that might be of importance in view of the current debate about seismic dynamics models [7,18,19].

II. EXPERIMENTAL STUDY

A. The friction setup

A schematic representation of the experimental setup is shown in Fig. 1. The setup is supported by a thick massive duralumin frame. The two surfaces in contact are made of 2-mm-thick Bristol board [20]. We have selected this unusual system because a number of tests on various materials (including ground metals) showed it to give the most regular dynamical behavior, reproducible at constant hygrometry on several hundreds of runs. This enables us to perform an extensive and precise study of the dynamical behavior. We attribute the high stability to the weakness of wear effects (as compared, for example, with metals). The regularity of the dynamical behavior (see Fig. 3) we believe to result from the fact that the cardboard layer retains enough large-scale adaptability to avoid large fluctuations in the number of contacts between the surfaces, which might arise from long wavelength undulations of the base metal substrates.

The lower (fixed) surface, which we will call the track, is glued with cyanoacrylate on the base frame. Depending on the range of V investigated, we have used track lengths of 20 cm to 1 m. The 10×10 cm^2 top moving surface (hereafter referred to as the slider surface) is glued by the same means onto a 1-cm-thick duralumin plate of the same lateral dimensions. Its mass—300 g— can be increased at will by adding calibrated masses atop. The slider is driven by a motor. The needed translation
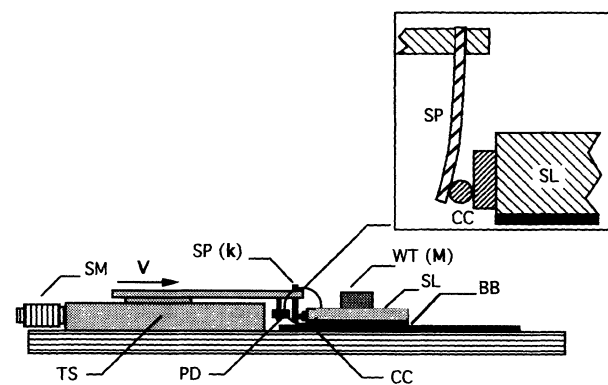

FIG. 1. Low-velocity friction setup (10^{-2} μm s^{-1} $< V < 10^3 \mu$m s^{-1}). BB, Bristol board; CC, crossed cylinders contact; PD, position detector; (SL, slider; TS, translation stage; SM, stepping motor; SP, cantilever spring of stiffness k; WT, calibrated weights. The mass of SL plus WT is M. In the high-velocity version (10^2 μm s^{-1} $< V < 5 \times 10^4$ μm s^{-1}), the brass cantilever spring (SP) is replaced by a helicoidal steel spring. The inset shows a magnified detail of the crossed cylinders contact between the bent cantilever spring (SP) and the slider (SL).

range of course scales with V. Typically, the slider total displacement in an experimental run ranges from a few millimeters when $V \approx 1~\mu\mathrm{m~s}^{-1}$ to 1 m for V approximately equal to a few $\mathrm{cm~s}^{-1}$. This large dynamic range has led us to use two different driving systems covering overlapping V ranges. At low and medium speeds (10^2 $\mu\mathrm{m~s}^{-1} < V < 10^3~\mu\mathrm{m~s}^{-1}$) we use a commercial translation table (Micro-Control UT50) including a geared down stepping motor. The resulting translational motion shows smoothed steps with a characteristic length of 0.1 $\mu\mathrm{m}$. Its total travel range is 20 mm. This limitation has led us to use at higher velocities (10^2 to $5 \times 10^4~\mu\mathrm{m~s}^{-1}$) a different setup: a geared down ac motor with velocity regulation provided by feedback from an optical encoder drives a capstan. This in turn drives a stranded steel cable, which pulls the slider. In both the low- and high-velocity setups, the driving system is coupled to the slider via a spring, the (adjustable, see below) stiffness of which, k, is always much weaker than that of the rest of the driving system. So k is the effective stiffness of the driving machine.

Both configurations give rise to specific noise problems, the extrinsic noise of the system having two kinds of origin:

(i) Motor-induced or accidental external mechanical perturbations, mostly in the audio range. We have measured the corresponding peak-to-peak vertical slider acceleration $\Delta\gamma$ in the bandwidth 0.2 Hz–5 kHz (with the motor on and off). At velocities $V < 100~\mu\mathrm{m~s}^{-1}$, $\Delta\gamma/g < 2.5 \times 10^{-3}$. The corresponding peak-to-peak vertical displacements were less than 0.1 $\mu\mathrm{m}$. The noise level for this setup increases at larger velocities ($> 10^2$ $\mu\mathrm{m~s}^{-1}$). In this latter range and above, the high-V setup, for which $\Delta\gamma/g < 2 \times 10^{-3}$, becomes preferable.

(ii) Large-scale (mm to cm) spatial inhomogeneities of the track. The larger V, the more relevant this type of noise becomes. Indeed, a precise determination of the bifurcation curve demands to wait for good stationarity. In practice, the corresponding signals must extend over tens of SS periods. This entails that the necessary track length increases with V (and with k^{-1}), thus more inhomogeneities are encountered. These inhomogeneities lie in fixed (reproducible) regions of the track. They give rise to variations in the stationary $\mu_d(V)$, which we have used as a test to determine which parts of the track are most homogeneous. These are the regions that we preferentially used for low-V experiments.

In the low-velocity setup, the elastic coupling between the driver and the slider is provided by a series of brass cantilever beam springs (see Fig. 1) of fixed length (30 mm), and variable thicknesses (0.5–3 mm) and widths (5–30 mm), with stiffnesses ranging from 10^2 to 10^6 $\mathrm{N~m}^{-1}$. In the high-velocity setup, k values from 10^2 to $5 \times 10^3~\mathrm{N~m}^{-1}$ are obtained with helicoidal steel springs. We have arbitrarily limited slider masses to 3 kg as a precaution against possible damage to the setup.

In order for experimental conditions to be well defined and reproducible, it is essential for the slider to retain enough degrees of freedom to settle, under its own weight, on the track surface and adjust to possible long-wavelength undulations. At the same time the spring-

slider translational coupling must be stable and very stiff. These conditions are met using a crossed-cylinders contact. A first, 1-mm-diam steel cylinder is glued with cyanoacrylate to the free end of the cantilever, a second, identical one is glued to the side of the slider. They meet by a compressive contact located about 1 mm above the sliding surface so as to minimize the couple felt by the slider. We have checked that the total equivalent stiffness of the spring-free driving stage is much larger than that of the stiffest cantilever used with a given driving setup, and that no viscoelastic relaxation of the glue was detectable. The tangential (shear) force on the slider is deduced from the measure of the displacement of the free cantilever (or spring) end, performed with an eddy-current commercial displacement gauge [21]. The noise level of the gauge plus amplifier is $10^{-2}~\mu\mathrm{m}$, its stability is $10^{-2}~\mu\mathrm{m}$ per minute, and its response bandwidth is better than 10 kHz.

As already mentioned, Bristol was selected from a variety of nonmetallic materials for the high regularity and reproducibility of its friction dynamics. These are a prerequisite for a meaningful exploration of a large region of parameter space. Stability is reached, for a given slider-track set, after a few runs; it then persists for hundreds of runs. The relative humidity was constant to within 5% about an average of 40%. When observed with an optical microscope, the surfaces, which are made of cellulose fibers, with diameters of order 10 $\mu\mathrm{m}$ and strongly glued together, show no sign of anisotropy.

B. Experimental results

When exploring the k-V space (see Fig. 2) in the above-mentioned ranges, two kinds of dynamical behaviors are observed. The corresponding k-V regions
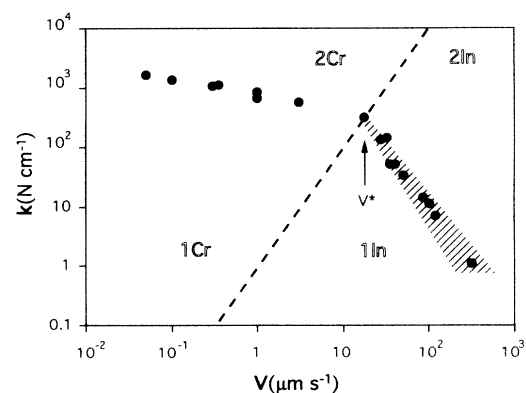

FIG. 2. Dynamical phase diagram in k-V space, measured for a loading mass $M = 1.2$ kg. Dots indicate the location of the bifurcation between stick-slip dynamics (region 1) and steady sliding (region 2). The dashed line separates the creep region (Cr) from the inertial one (In). It crosses the bifurcation curve at $V = V^*$ (see text). The dots in (Cr) show the location of the continuous Hopf bifurcation. The existence of hysteresis in (In) is symbolized by the hatched zone; in this region, dots refer to the first intermittencies observed when increasing V (see text).
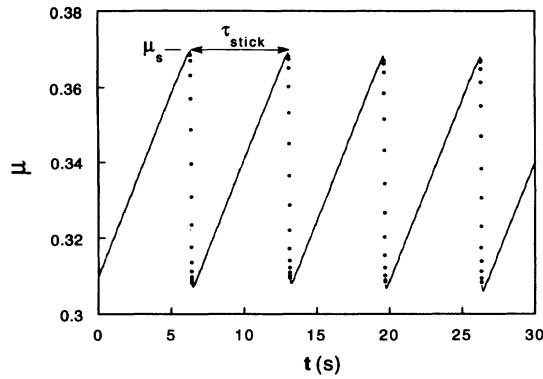
FIG. 3. Normalized friction coefficient $\mu = F/Mg$ vs time recording in the stick-slip regime (region 1 of Fig. 2). $M = 2.1$ kg; $k = 1.5 \times 10^4$ N m^{-1}; $V = 10$ μm s^{-1}. During the stick, μ increases linearly. The slip time $\tau_{slip} = 3.8 \times 10^{-2}$ s. Data corresponding to the slip are marked by circles for the sake of clarity.

are separated by a bifurcation curve $k_c(V)$ [or $V_c(k)$]. Stick-slip occurs in zone (1) below the bifurcation curve. It is highly periodic, as illustrated in Fig. 3. In zone (2)—high V and/or high k—the slider moves steadily at the pulling velocity V. It is in this regime that we are able to measure a coefficient of *stationary* kinetic friction $\mu_d(V)$. Its stability and reproducibility are a good test of track heterogeneity and/or aging. Note that any V can, in principle, be reached by using a stiff enough spring $[k > k_c(V)]$.

1. Friction coefficients

As a characterization of the tribological properties of the system, we have measured the static and kinetic

coefficients of friction.

(i) The stationary kinetic friction coefficient μ_d is found to depend on the steady sliding velocity V (Fig. 4). When it is measured in the low-velocity part of region 2 (Fig. 1), μ_d decreases with increasing V and can be fitted by the expression

$$\mu_d(V) = a_v - b_v \ln(V/V_0) , \quad a_v = 0.369 , \quad b_v = 0.014$$

$$(\text{with } V_0 = 1 \ \mu\text{m s}^{-1}) . \quad (6)$$

This logarithmic behavior spans over three decades. In the high-velocity part of region 2, $\mu_d(V)$ becomes an increasing function of V which, in first approximation, can be described by a linear function extrapolating, for $V \to 0$, to a finite positive value μ_{d0}.

(ii) The static threshold μ_s is found to depend on the "stick time" τ_{stick} prior to motion. This dependence can be observed following two procedures: the static friction coefficient μ_s can be measured directly, the system being left at rest under zero shear for an aging time τ_{stick}, the shear being then ramped up on a time much shorter than τ_{stick} to a value where sliding occurs. Alternatively, we can extract μ_s from stick-slip force recordings in zone 1, τ_{stick} being there the loading time before slip (Fig. 3). Note that this last operational definition assumes that $\mu_s(\tau_{stick})$ is not affected by an increase of the shearing force during the loading stage. The first procedure is suitable for large values of τ_{stick} (typically $\tau_{stick} > 10$ s) while using stick-slip allows stick times of order 1 s to be reached. The results obtained by both procedures agree for a significant overlapping time region. The corresponding results are shown in Fig. 5. They are reasonably well fitted by expression (3) with
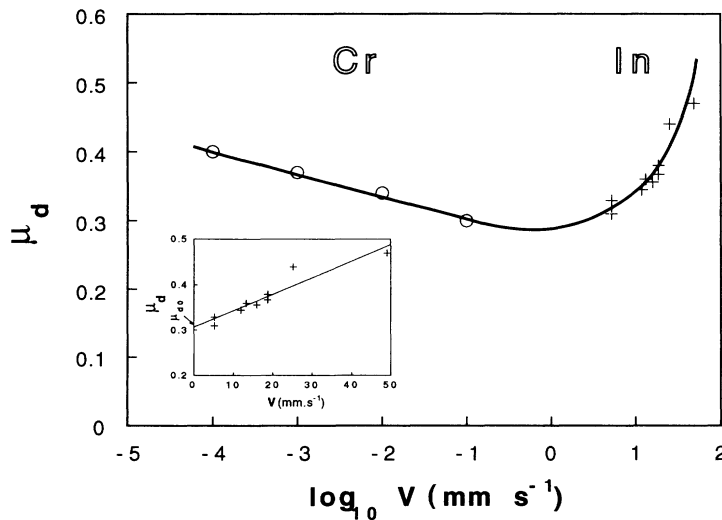

FIG. 4. Dynamic friction coefficient μ_d vs the logarithm of the pulling velocity V in the steady sliding regime (main figure). Data for $V > 1$ mm s^{-1} (crosses) have been obtained with $k = 5 \times 10^2$ N m^{-1} and advantage has been taken by working at decreasing V of the hysteresis of the bifurcation in the inertial regime at low noise. A linear fit of the data in the inertial regime (2In) is shown in the inset. Data for $V < 10^{-1}$ mm s^{-1} (circles) were obtained by working in region (2Cr) of Fig. 2. A line is drawn as a guide for the eyes.
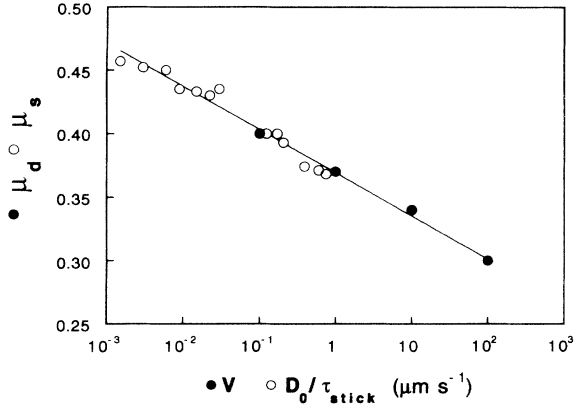
FIG. 5. Plot of the stationary dynamic friction coefficient μ_d vs velocity V (full dots), and of the static friction coefficient μ_s vs D_0/τ_{stick} (circles). The memory length value $D_0 = 0.9$ μm is obtained from the best logarithmic fit (full line).

$$a_s = 0.370 \ , \quad b_s = 0.015 \quad \text{(with } \tau_{\text{stick}} \text{ in seconds) .} \tag{7}$$

Thus $b_v = b_s = 0.0145 \pm (5 \times 10^{-4})$ and (6) together with (7) leads us to define a length D_0 by

$$\ln D_0 = \frac{a_v - a_s}{b_s} \ , \tag{8}$$

so that relation (4) holds. The corresponding plot is shown in Fig. 5. From (6) and (7) we obtain

$$D_0 \approx 0.9 \ \mu\text{m} \ .$$

The emergence of a characteristic, mesoscopic length naturally leads, following Rabinowicz [12] and Scholz [3], to the notion of an average "contact size" on which the system retains a memory of its detailed contact structure. The experimental law (4), which relates static and kinetic data for a single system, may be connected to the idea, first inferred by Scholz [16] from scattered data on rocks, that static evolution and slow frictional dynamics result from the same physical process, namely, creep of the contact spots under normal or tangential loading.

2. The creep regime

a. Evidence of creep motion. Figure 3 displays a typical force recording in the stick-slip zone 1, far enough from the bifurcation line. The normalized force $\mu(t) = F(t)/Mg$ increases linearly for a stick time τ_{stick}. The slip appears as a quasidiscontinuity over a time τ_{slip} ($\ll \tau_{\text{stick}}$) of the order of the inertial time $\tau_{\text{in}} = 2\pi (M/k)^{1/2}$.

However, looking in more detail to the signal, a deviation from linearity in the "stick" part of the cycle may be noticed. This deviation is small compared to the slip amplitude, and in practice, the dynamical range of the force transducer limits its observability. This limitation can be

circumvented by monitoring directly the displacement $x(t)$ of the slider with respect to the track. A perfect stick corresponds then to $x(t) \equiv 0$. A typical recording of $x(t)$ is shown in Fig. 6(a): departure from perfect stick increases nonlinearly with time and is mostly visible before the rapid slip event. This corresponding slow motion will be called creep; it has already been observed in rock mechanics experiments, where it was named "precursory stable sliding" [3].

An unambiguous distinction between creep and slip is possible provided that time scales for these two processes are well separated. A first characteristic of the function $x(t)$ is then D_1, defined as the distance crept before slipping [Fig. 6(a)]. D_1 is found to lie in the micrometer range. Experimentally, $x(t)$, hence D_1, show no noticeable dependence on k and M over the range of parameters investigated [Fig. 6(b)], in spite of the considerable disparity of sticking times involved. However, when varying the driving velocity V over decades, although $x(t)$ is found to be V dependent [Fig. 6(c)], Vt does not provide a simple scaling to $x(V,t)$ [Fig. 6(d)].

A second evidence of the creep process has been obtained from the study of stress relaxation at zero pulling velocity. The system is loaded up to a level $\mu = \mu_{\text{in}}$ below the slip threshold μ_s; the pulling system is then stopped, and the slow motion is studied by recording the time variation of the force. Figure 7 displays a typical example of the corresponding force signal.

The closer μ_{in} is to the static threshold μ_s, the larger the amplitude of the creep relaxation. In experiments with large amplitude, the signal-to-noise ratio is large and we are able to check unambiguously that, as is often the case in, e.g., plastic dynamics, the relaxation is nonexponential. This may be related to the fact that no characteristic time can be extracted either from the logarithmic variations exhibited by $\mu_s(t)$ or $\mu_d(V)$.

We find that the amplitude of the creeping relaxation increases markedly as the initial stress is raised towards the slip threshold. This must be related with the nonlinear acceleration of creep in the SS experiments as the slip event is approached. This is the signature of a self-accelerating dynamics close to a runaway threshold, an idea that will be developed in Sec. III. It agrees with the earlier-mentioned quasi-independence of the measured creep signal on the stick time.

The two above manifestations of creep motion remain small effects as long as the system is far from the bifurcation curve. For example, when performing the $\mu_s(\tau_{\text{stick}})$ determination, the error induced by creeping, $\Delta\mu_s/\mu_s \approx D_1 k/Mg\mu_s \ll 1$ for typical values of k/M. However, when approaching the bifurcation curve from below at low velocities, the nature of the dynamics changes. While, deep inside region 1, a slip process occurring on a time scale of order $\tau_{\text{in}} = 2\pi (M/k)^{1/2}$ is easily identified, the τ_{in} scale becomes irrelevant when the bifurcation is approached: inertial slip disappears (Fig. 8). Creep thus becomes the essential mechanism in the low-velocity part of the bifurcation curve.

As will be discussed below, a thoroughly different behavior is observed along the high-velocity part of the bifurcation curve. The existence of these two regimes we

interpret as follows. We define a creep time scale as $\tau_{cr} = D_0/V$. Note that we have found the *creep length* D_1 to be k and M independent and weakly V dependent with $D_1 \approx D_0$; so $\tau_{cr} \approx D_1/V$. On this basis, it is natural to define heuristically, in (k, V) space, two regions separated by the line $\tau_{cr} \approx \tau_{in}$: region (Cr), on the left side of this line, which corresponds to $\tau_{cr} > \tau_{in}$, is the creep-dominated region, and region (In), to the right, is the "inertial" region $(\tau_{cr} < \tau_{in})$. The dashed line in Fig. 2, which is drawn to cross the bifurcation curve at $V = V^*$, corresponds to $\tau_{cr} \approx 1.5\tau_{in}$.

b. The SS–steady sliding bifurcation. When performing a set of experiments described by a trajectory in parameter space that crosses from regions (1Cr) to (2Cr), we observe an evolution of the dynamics as shown in Fig. 8. As the bifurcation is approached from below, the SS amplitude decreases continuously towards zero on the bifur-

cation line, while a separation between (crept) stick and slip becomes increasingly difficult.

We are thus able to define, for a given M, a critical line in k-V space, $k_c(V)$ [or $V_c(k)$] defined by a vanishing amplitude of oscillations. The corresponding SS–steady sliding bifurcation is continuous and reversible.

Measurements for various M at given (k, V) show that the relevant parameter in this creep regime is actually k/M instead of k. Advantage was taken of this behavior to ease the precise determination of the bifurcation line: once a small SS amplitude had been obtained by rough adjustment of k and V, the bifurcation was reached by successive removal of small loading weights.

$(k/M)_c$ is found to be a slowly decreasing function of V. We find that a dependence of the form

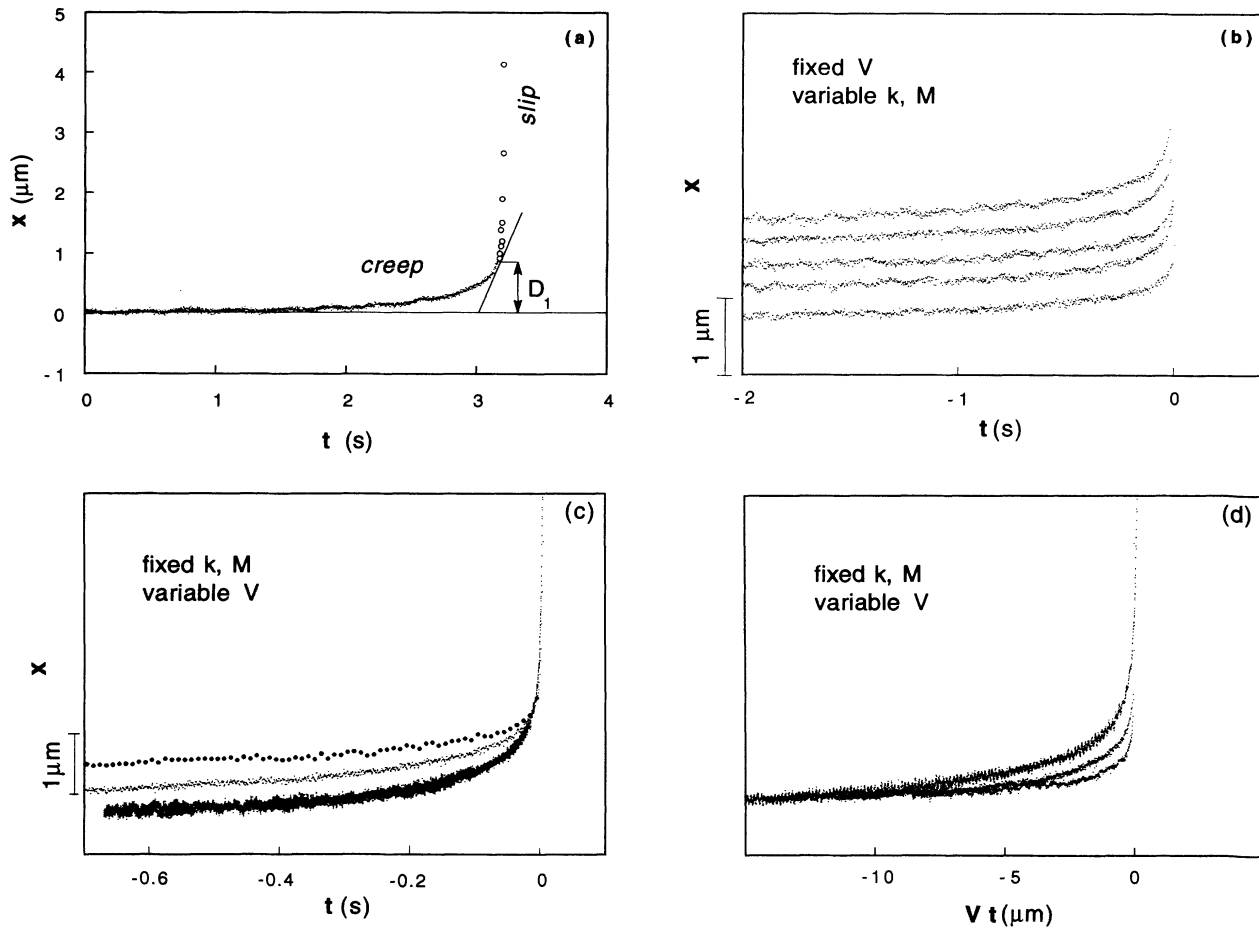$$(k/M)_c = (k/M)_{c0} - \alpha \ln(V/V_0) \qquad (9)$$

FIG. 6. (a) Direct measurement of the slider displacement x vs time t for $M = 0.32$ kg, $k = 1.5 \times 10^4$ N m^{-1}, $V = 5$ μm s^{-1} (Cr region of Fig. 2). The slider, initially at rest at $x = 0$ under zero tangential load ($\mu = 0$) is then pulled at constant velocity V. The tilted line has slope V. The creep length D_1 is defined as the value of x for which $\dot{x} = V$. Data corresponding to the subsequent slip event are marked by circles for the sake of clarity. The period of data acquisition is $\Delta t = 2 \times 10^{-3}$ s. Only the beginning of the slip is shown, the total slip displacement $\Delta x_{slip} \approx 20$ μm. (b) Creep displacement x vs time t for $V = 2.5$ μm s^{-1} and (from lower to upper curve) $k/M = 0.42$, 1.2, 0.69, 2.5, 4.5 ($\times 10^4$ s^{-2}). A vertical shift has been added to each curve for the sake of clarity. The shape of $x(t)$ is independent of the value of k/M. (c) Creep displacement x vs time t for $k/M = 7.1 \times 10^3$ s^{-2} and (from lower to upper curve) $V = 1$, 10, 50 μm s^{-1}. (d) Same data as (c), plotted vs Vt (the order of the curves is reversed). Both $x(t)$ and $x(Vt)$ are markedly V dependent.
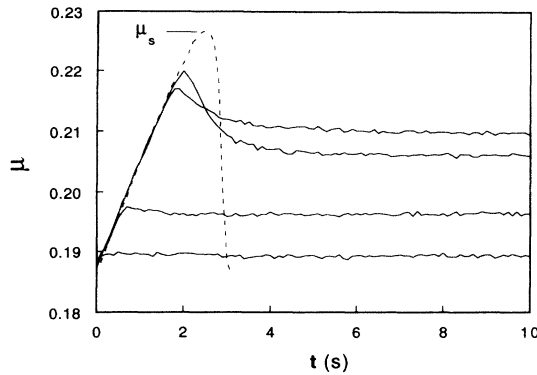
FIG. 7. Friction coefficient μ vs time in force-relaxation experiments. After being left at rest for a fixed time lap of 15 s at $\mu=0.15$ (not shown), the system is loaded up to an initial level μ_{in} at which the pulling machine is stopped. The static coefficient of friction μ_s is determined from the dashed curve which corresponds to ordinary stick-slip. Creep relaxation increases for decreasing $\mu_s - \mu_{in}$.
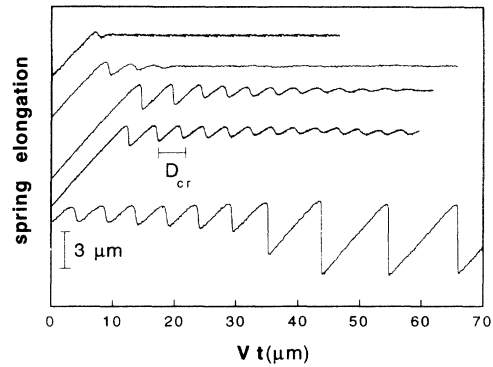

FIG. 9. Transient response of the system to a forward impulse at $t=0$. All curves correspond to $k=1.5\times10^5$ N m^{-1}. From upper to lower curve: $M=0.32$ kg, $V=6.0$ μm s^{-1}; $M=0.78$ kg, $V=1.4$ μm s^{-1}; $M=0.78$ kg, $V=0.57$ μm s^{-1}; $M=0.78$ kg, $V=0.31$ μm s^{-1}; $M=1.1$ kg, $V=0.9$ μm s^{-1}. $D_{cr}=VT_{osc}$ (see text) is indicated for one curve: here $D_{cr}=4.4$ μm. Note that the two lowest curves reach stationary oscillating states of finite amplitude (Fig. 8).

with $\alpha=1.8\times10^4$ s^{-2}, $(k/M)_{c0}=7.2\times10^4$ s^{-2} and $V_0=1$ μm s^{-1} is reasonable. Given that our data only cover two decades of V, this functional form should only be considered as a tentative one.

The nature of the bifurcation was analyzed by studying the response of the system to pulling perturbations, namely, a forward impulse given to the slider (Fig. 9). The typical response is oscillating and damped. We conveniently measure the pseudoperiod of the oscillations T_{osc} and the damping time T_{damp}. Far above the bifurcation line in (2Cr), the response is aperiodic. When approaching the bifurcation line, T_{damp} diverges while T_{osc} remains at a finite value. On the line, the response becomes a pure oscillation of period $T_{osc}[(k/M)_c]$. The response on the SS side of the line is studied as follows: Starting from a point close to the bifurcation in (2Cr), we add a loading weight (or decrease V) so as to reach a point in (1Cr). The initial steady sliding state is unstable,
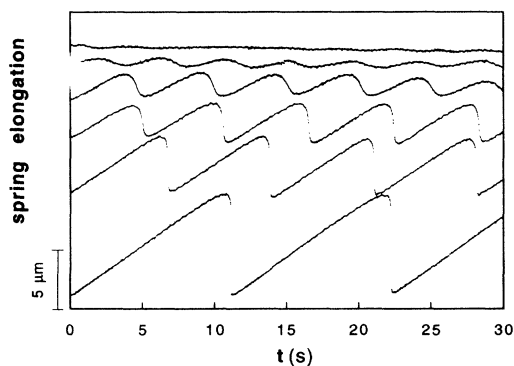

FIG. 8. Evolution of the amplitude of the steady-state oscillations, when approaching the bifurcation from region (1Cr) of Fig. 2. $V=0.9$ μm s^{-1} $k=8.8\times10^4$ N m^{-1} and (from lower to upper curve) $M=1.2$, 0.745, 0.695, 0.670, 0.640, 0.620 kg.
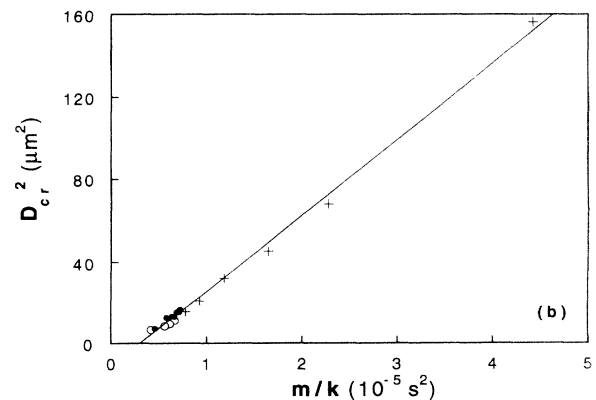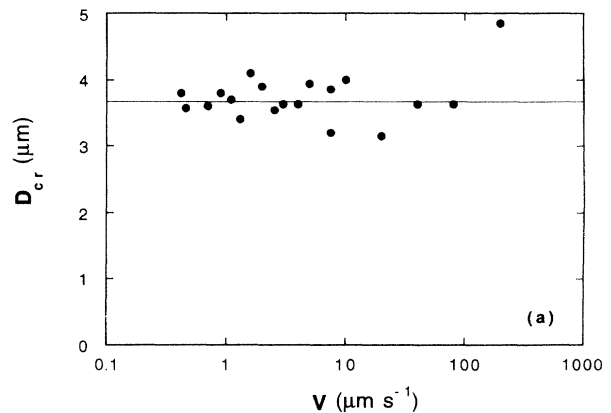

FIG. 10. (a) Pseudodistance $D_{cr}=VT_{osc}$ (see text) vs pulling velocity V for $k=8.2\times10^4$ N m^{-1} and $M=0.37$ kg. The solid line is set at the mean value of the data. Note the log scale for V. (b) D_{cr}^2 vs M/k along three different paths in region (2Cr): along the bifurcation curve (crosses); at $V=2.3$ μm s^{-1}, $k=8.2\times10^4$ N m^{-1} and M ranging from 0.37 to 0.59 kg (dots); $V=0.25$ μm s^{-1}, $k=1.5\times10^5$ N m^{-1} and M ranging from 0.62 to 1.0 kg (circles).

and SS settles via an amplifying oscillatory transient ultimately saturating into the SS cycle. The amplification time of the transient diverges also at the bifurcation. All these features permit us to conclude that the bifurcation from SS to steady sliding is of the direct Hopf type.

c. Variations of $T_{\text{osc}}(V,k/M)$. We have investigated the variations of the pseudoperiod of crept relaxation T_{osc} with the mechanical parameters of the system.

(i) No variation of $D_{\text{cr}} = VT_{\text{osc}}$ with V can be measured over more than two decades [Fig. 10(a)].

(ii) D_{cr} is found to depend on k/M [Fig. 10(b)] though remaining within the range 1–10 μm. So, $T_{\text{osc}} = D_{\text{cr}}(k/M)/V$.

d. Experimental length scales. Up to this point, in the creep zone (Cr), either in the SS or the steady sliding regime, we have encountered three distances, namely, D_0, D_1, and D_{cr}. All of them are in the micrometer range but each presents a particular flavor. Since D_{cr} depends on k, it is obviously not a characteristic of the sliding contact alone; the V dependence of D_1 indicates that this is a dynamical quantity while D_0 seems to be more intrinsically related to the properties of the material. There is no reason to expect the three distances to be simply related.

C. Crossover toward the inertial regime

The former creep bifurcation is observed up to $V \approx 100$ μm s^{-1}. For larger driving velocities, the nature of the bifurcation is deeply modified.

(i) The transition occurs at finite amplitude of the SS oscillations.

(ii) It gives rise to either hysteresis or temporal intermittency, depending on the noise level of the system (see Sec. II A). For a low-noise system, the transition "steady sliding→SS" occurs at a velocity markedly lower (up to a 10:1 ratio) than the "SS→steady sliding" one. The resultant hysteresis loop narrows when increasing the noise level, ultimately giving rise to temporal intermittencies within the reduced hysteretic range; they consist in an alternation of variable numbers of periodic SS cycles and of steady slidings of random duration. As V is increased at constant k and M, the relative duration of steady sliding increases, and perfect steady sliding finally sets up.

(iii) Indeed, in the hysteretic region, we find that it is possible, with the help of tailored perturbations, to induce the system to switch from one stability branch to the other, and this in both directions: SS→steady (steady→SS).

These features strongly suggest that the transition should be analyzable, at least globally, as an inverted bifurcation. Such an interpretation is, in particular, compatible with the appearance of intermittencies at high noise levels.

Whatever the dominant behavior, we can no longer define a clear-cut bifurcation line but, at best, a transition zone. This corresponds in Fig. 2 to the hatched zone of the (1-2) separation line. In this region, we have not been able to ascertain whether or not the combination k/M (rather than k, M separately) remains the only relevant inertial parameter, due to the above-mentioned loading weight limitations and to transition width effects.

In this region, the average $|dk_c/dV|$ at constant M is much larger than in the creep region. So, a quite well-localized crossover can be identified for V^* and $(k/M)^*$. It is worth noting that for the crossover values, the relation $\tau_{\text{cr}} = \tau_{\text{in}}$, defined earlier as separating the creep-dominated from the inertia-dominated regimes, is roughly fulfilled (see Fig. 2). Moreover, the value V^* corresponds also approximately to the crossover between velocity-weakening and velocity-strengthening behavior of the stationary kinetic friction coefficient $\mu_d(V)$ (Fig. 4). These two experimental observations will be connected in Sec. III.

III. A HEURISTIC MODEL

A. Physical basis

The main results of the experimental study presented above can be summarized as follows:

(i) Sliding at low velocities—typically in the μm/s range—is primarily controlled by a creep process.

(ii) The time dependence of μ_s gives evidence that the physical contacts between the solids undergo a slow relaxation process.

(iii) The fact that $\mu_s(t)$ and $\mu_d(V)$ satisfy relation (4) indicates the existence of a memory length. This may be interpreted as when the slider has moved by D_0 relative to the track, the population of contacts has been destroyed and renewed.

(iv) The frictional dynamics crosses over from creep controlled to inertia controlled when $\tau_{\text{cr}} \approx \tau_{\text{in}}$. One of the manifestations of this crossover is the change of the steady $\mu_d(V)$ from slip weakening to slip strengthening.

These results were obtained from an extensive and reproducible study of a single physical system. (i) to (iii) agree with earlier conclusions deduced from metal and rock studies, to which they provide strong confirmation, on a system (paper on paper) of a very different physical structural and chemical nature.

So, creep, aging, and the existence of a memory length appear as stable characteristics of the dynamics of slow friction between macroscopic solid surfaces, i.e., surfaces with a large population of contacts with lateral dimensions in the micrometer range. Result (iv), though concerned with a still unreported effect, we also believe to be quite general.

We now want to build a model for the motion of the experimental system studied in Sec. II above as simple as possible while capturing these physical features. For the sake of simplicity, we forget here the internal elastic degrees of freedom of the slider, the motion of which we assume to reduce to the one-dimensional motion of its center of mass G along the pulling direction x.

Let $x(t)$ be the instantaneous position of G, moving due to the force F_{ext} imposed by a spring (k) of instantaneous elongation $x_0(t) - x(t)$, and subject to a shearing frictional force F_{fr}. Standard models assume that the system, initially at rest, remains motionless as long as $|F_{\text{ext}}| < Mg\mu_s$, and that when the system is moving $F_{\text{fr}} = Mg\mu_d\{\dot{x}(t)\}$, where $\mu_d(V)$ is the steady kinetic friction coefficient, exhibiting slip weakening at small V or an abrupt discontinuity $[\mu_d(0^+) < \mu_s]$.

It is immediately clear that such models are incompatible with our low-V results. For example, they exclude slow relaxation under stresses below the μ_s threshold, and they are incompatible with stable steady sliding in the slip-weakening range, contrary to what we observe.

These remarks, added to results (i)–(iv), lead us to think that the standard description must be modified so as to take into account two distinct physical processes.

(1) The first one is creep, which is controlling up to a threshold, corresponding, for example, to a rather abrupt switch from creep to slip dynamics observed during SS cycles deep inside region (1Cr). Following Eyring, Glasstone, and Laidler [22,23], we will assume that the creep process is a thermally activated motion in a potential modulated in space. In models of bulk thermal creep the modulations are naturally associated with the underlying crystal structure. Here we assume them to describe phenomenologically a pinning effect related to surface inhomogeneities (roughness) on the mesoscopic (micrometer) scale. Again, for the sake of simplicity, we assume this pinning potential U to be periodic along x, with period a and amplitude modulation ΔU_0 [Fig. 11(a)].

This pinning effect certainly only affects the very limited part of the slider which effectively takes part in the plastic processes by which real contacts deform and get destroyed. This "creeping volume" we can imagine, in a crude first approximation, to be coupled quasirigidly to the main part of the slider, which then acts as a thermal bath into which energy can be dissipated by acoustic radiation, and as a rigid transmitter of the external pulling force. We will call N_{cr} the number of moles in the creep-

ing volume; more exactly, $N_{cr}N_{Avogadro}$ is the number of degrees of freedom involved in the creep process.

So, N_{cr} is an *a priori* unknown quantity, the order of magnitude of which we will try to extract from experimental data. Note that, if one makes the reasonable assumption that it is proportional to the total area of real contact, the Bowden-Tabor interpretation of Amontons's law leads one to expect it to scale with the total mass M of the slider.

The driven system thus moves in the total potential $U_{eff} = U + V_{ext}(x, t)$, where

$$V_{ext}(x,t) = -\int^x F_{ext}(x,t)dx = \frac{k}{2}\{x - x_0(t)\}^2 . \tag{10}$$

For small external F_{ext}, U_{eff} retains a modulated structure on top of a slow parabolic variation which can be approximated locally by an average slope [see Fig. 11(b)] provided that $a \ll |x - x_0|$. Let us assume, for the moment, that x_0 is fixed, and that the representative point of the system lies in the vicinity of a minimum of U_{eff}.

Creep out of this minimum is due to thermal fluctuations, which can be described by a Langevin δ-function-correlated random force $R(t)$. This immediately and necessarily entails that the system is also submitted to an average frictional force $(-\Gamma\dot{x})$, related to the fluctuating one by the fluctuation-dissipation theorem

$$\Gamma = \frac{1}{2k_B T}\int_{-\infty}^{\infty} \langle R(0)R(t)\rangle dt . \tag{11}$$

Note that this frictional force is necessarily slip strengthening $(\Gamma > 0)$. $R(t)$ and Γ account for the coupling of the sliding interface with the vibrational degrees of freedom of the two solids. We assume them to be x-independent, thus neglecting again statistical fluctuations due to medium- or large-scale interface inhomogeneities. So, the dynamical equation describing the system reads

$$M\ddot{x} + \Gamma\dot{x} = -\frac{\partial U_{eff}}{\partial x} + R(t) . \tag{12}$$

(2) We now want to insert, into this description, the effect of the slow aging of contacts, and the existence of a finite memory length D_0. For this purpose, we define a phenomenological variable, $\phi(t)$, which we call the contact age, by

$$\phi(t) = \int_{t_0}^{t}\exp\left\{-\frac{x(t) - x(t')}{D_0}\right\}dt' , \tag{13}$$

where t_0 is the time at which the two solids first came into contact. Equation (13) is equivalent to

$$\dot{\phi} = 1 - \frac{\dot{x}}{D_0}\phi \tag{14}$$

with initial condition $\phi(t_0) = 0$.

Such a definition is directly inspired by Ruina's [10,11] description in terms of a constitutive variable. However, it improves upon it by allowing for a reasonable interpolation between the system at rest, for which $\phi(t) = t - t_0$, (i.e., the age at rest is simply the duration of the solid-
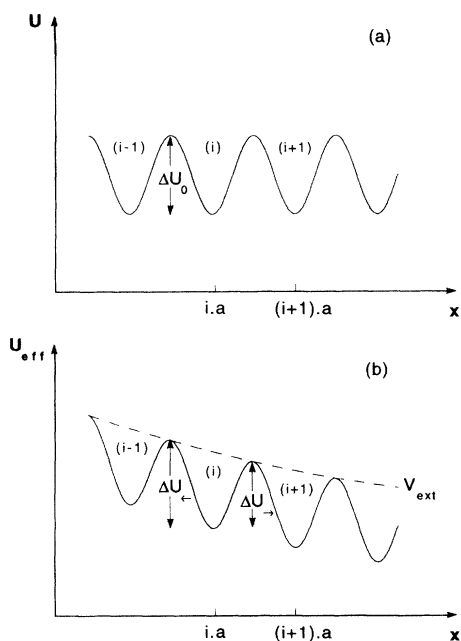

FIG. 11. Typical shape of pinning potential (a) in the absence, and (b) in the presence of the external shearing force F_{ext}. "i" labels the "pinning centers."

solid contact) and motion at constant velocity V, for which

$$\phi_{\text{stat}} \equiv \phi_{\text{stat}}(V) = \frac{D_0}{V} .$$ (15)

That is, Eq. (15) expresses the idea formulated from result (iii) above that D_0 is the average shearing displacement necessary to break a typical contact by brittle or ductile fracture.

We now introduce the physical effect of aging by assuming that the older the contacts, the stronger the pinning, i.e., the larger the height modulation ΔU_0 of the pinning potential U:

$$\Delta U_0 \equiv \Delta U_0(\phi) ,$$ (16)

where $d(\Delta U_0)/d\phi > 0$. The frictional dynamics in the low-velocity regime is therefore, finally, described by Eqs. (14) and (15) for the two variables x and ϕ, where now

$$U_{\text{eff}} = U(x,\phi) + V_{\text{ext}}(x,t) .$$ (17)

B. Dynamics in the creep regime

Brownian motion for a single degree of freedom, driven at constant bias in a time-dependent potential, has been analyzed in great detail by many authors. Several regimes must be distinguished [24,25] depending on whether (a) the mechanical motion in U_{eff} is over or underdamped (these two limits correspond to $\Gamma \gg M\omega_0$ and $\Gamma \ll M\omega_0$, where ω_0 is the oscillation frequency about one of the minima of U_{eff}), and (b) the average energy δE lost by the system while moving from one maximum of U_{eff} to the vicinity of the next one is large or small compared with the thermal energy $N_{\text{cr}}RT$—with N_{cr} the number of moles involved in the creep motion. In all cases, one can distinguish between:

(i) A pinned regime, at low imposed external force ($\Delta U_0 \gg N_{\text{cr}}RT$), where the system undergoes a thermally activated creeping motion. Its velocity is given by

$$\dot{x} = a \left\{ \frac{1}{\tau_\rightarrow} - \frac{1}{\tau_\leftarrow} \right\} ,$$ (18)

where $\tau_\rightarrow$ ($\tau_\leftarrow$) is the thermal time for escaping from a given well into its downstream (upstream) nearest neighbor. Let $\Delta U_\rightleftarrows$ be the corresponding barrier heights [see Fig. 11(b)]:

$$\frac{1}{\tau_\rightleftarrows} = C \exp \left\{ - \frac{\Delta U_\rightleftarrows}{N_{\text{cr}}RT} \right\} .$$ (19)

(ii) A freely sliding regime, at large external driving force. The limit of very strong bias simply corresponds to ordinary stable frictional motion, i.e.,

$$\dot{x} = F_{\text{ext}}/\Gamma .$$ (20)

The two regimes are separated by a "runaway threshold," which characterizes the order of magnitude of the external force at which the thermally fluctuating system gets depinned from the modulations of U.

Both the value of this threshold and the prefactor in Eq. (19) depend on the energy loss and damping conditions. In the absence of a microscopic model, we will assume, in order to fix ideas, that the system operates in the so-called Eyring's absolute rate regime [23,25], which corresponds to

$$\Gamma \ll M\omega_0 , \quad \delta E \gg N_{\text{cr}}RT .$$ (21)

This assumption, which we borrow from Nozières's discussion of desorption dynamics [25], is by no means crucial for the following analysis, the results of which would retain the same qualitative features in the other regimes.

Under conditions (21), one obtains

$$C = \frac{\omega_0}{2\pi} ,$$ (22)

and the runaway threshold is defined by the condition

$$\Delta V_{\text{ext}} \gtrsim \delta E \approx \frac{\Gamma}{M\omega_0} \Delta U_0 ,$$ (23)

where ΔV_{ext} is the potential drop between two neighboring maxima of U_{eff} associated with the external force. Finally, note that, as soon as $\Delta V_{\text{ext}} \gg N_{\text{cr}}RT$, upstream escape is negligible with respect to the downstream one, and $1/\tau_\leftarrow$ can be neglected in Eq. (18).

Expressions (18) and (19) for the creep mobility are valid for a system submitted to a time- and position-independent external force and pinned by a time-independent potential $U(x)$. The spring-driven slider experiences a pulling force F_{ext} that depends on both x and t, via the spring elongation $x_0(t) - x$. On the other hand, the aging effect results in a time dependence of U via Eq. (16). Results (18) and (19) should, in principle, be modified so as to take into account the variations of U and F_{ext} on the average length ($\Delta x \sim a$) and duration ($\Delta t \sim \tau_\rightarrow$) of an average escape event. Since these quantities depend on time through the, a priori, unknown evolution of the dynamical variables x and ϕ themselves, this poses by itself quite a formidable problem of coupled nonlinear and Brownian dynamics, the solution of which should result in a renormalization of barrier heights and of the runaway threshold. In the present preliminary model, we circumvent this problem by assuming that the corresponding variations are small enough for an adiabatic approximation to be valid, i.e., that $\{a, \dot{x}_0(t)\tau_\rightleftarrows\} \ll |x_0(t) - x|$ and $\tau_\rightleftarrows |\partial \ln \Delta U_\rightleftarrows/\partial t| \ll 1$.

So, in the creep regime, the instantaneous sliding velocity, at time t, is given by Eqs. (18), (19), and (22) where ΔU is understood to take on its value at the same time, as well as ω_0, which should also depend on ϕ, insofar as $U(x)$ does. We then obtain, from Eqs. (18), (19), and (22), in the creep regime $\Delta V_{\text{ext}} \ll (\Gamma/M\omega_0)\Delta U_0$

$$\dot{x}(t) \cong \frac{\omega_0 a}{2\pi} 2 \sinh \left\{ \frac{ka\{x_0(t) - x\}}{2N_{\text{cr}}RT} \right\} \exp \left\{ - \frac{\Delta U_0(\phi)}{N_{\text{cr}}RT} \right\} .$$ (24)

So, as soon as the work performed by the driving force when moving from a minimum of U to the next max-

imum is much larger than the thermal energy $N_{cr}RT$, Eq. (24) can be inverted into

$$F_{ext}(x,t) = \frac{2}{a} \left\{ \Delta U_0(\phi) + N_{cr}RT \ln \left| \frac{2\pi \dot{x}}{\omega_0 a} \right| \right\} . \quad (25)$$

1. Steady sliding

Let us now consider the case of stationary sliding in the creep regime. In this case, F_{ext} becomes a t- and x-independent constant, and (25) directly provides the expression of the stationary kinetic friction force as measured in the experiments of region (2Cr) of Fig. 2. Making use of expression (15) for ϕ_{stat}, we obtain

$$\frac{2}{a} \left\{ \Delta U_0(\phi) + N_{cr}RT \ln \left| \frac{2\pi D_0}{\omega_0 a\phi} \right| \right\} = Mg\mu_d \left\{ \frac{D_0}{\phi} \right\} , \quad (26)$$

where the functional form of $\mu_d(V)$ for our system is given by expression (6). So, up to corrections that may arise from the ϕ dependence of ω_0,

$$\Delta U_0(\phi) = \Delta U_{00} + \beta \ln(\phi/\phi_0) \quad (27)$$

with

$$\beta = aMgb_v + N_{cr}RT . \quad (28)$$

Expression (27) can be qualitatively understood as describing the increase in contact strength associated with the slow plastic relaxation implied by the interpretation of Bowden and Tabor [1]. So, Eq. (25) can be rewritten as

$$k\{x_0(t) - x\} = Mg\mu_d \left\{ \frac{D_0}{\phi} \right\} + \frac{2N_{cr}RT}{a} \ln \frac{\dot{x}\phi}{D_0} . \quad (29a)$$

The nonlinear friction dynamics in the creep regime is now completely specified by Eq. (29a) together with Eq. (14), which we rewrite here for the sake of clarity:

$$\dot{\phi} = 1 - \frac{\dot{x}}{D_0}\phi . \quad (29b)$$

2. The SS — steady sliding bifurcation

We now want to study the linear stability of the above steady sliding motion. We set

$$\phi = D_0/V + \delta\phi \exp(\Omega t) ,$$

$$x = Vt - \Delta x_{st} + \delta x \exp(\Omega t) , \quad (30)$$

and expand Eqs. (29a) and (29b) to first order in $\delta\phi, \delta x$. Noticing that

$$\left| \frac{\partial}{\partial \phi} \mu_d \left\{ \frac{D_0}{\phi} \right\} \right|_{\phi = D_0/V} = -\frac{V}{D_0} \frac{d[\mu_d(V)]}{d[\ln V]} , \quad (31)$$

we obtain the following dispersion relation for the rate of growth of fluctuations about steady sliding:

$$\left\{ \frac{\Omega}{V} \right\}^2 + \lambda \left\{ \frac{\Omega}{V} \right\} + \frac{ak}{2N_{cr}RTD_0} = 0 , \quad (32a)$$

where

$$\lambda = \frac{a}{2N_{cr}RT} \left\{ k + \frac{Mg}{D_0} \frac{d[\mu_d(V)]}{d[\ln V]} \right\} . \quad (32b)$$

The roots of Eq. (32a)

$$\frac{\Omega_{\pm}}{V} = -\frac{\lambda}{2} \pm \frac{1}{2} \left[\lambda^2 - \frac{2ak}{N_{cr}RTD_0} \right]^{1/2} \quad (33)$$

are real negative at very large k. The steady sliding state becomes linearly unstable when $\lambda < 0$, i.e., for

$$k \leq k_c(V) = -\frac{Mg}{D_0} \frac{d[\mu_d(V)]}{d[\ln V]} . \quad (34)$$

Since $\mu_d(V)$ exhibits a slip-weakening behavior in the low-velocity range, $k_c(V)$ is a positive quantity. That is, we recover here the results provided by the zero-inertia limit of Ruina's theory, his constant A being given here by

$$A = 2N_{cr}RT/a . \quad (35)$$

Since the bifurcation occurs for $\lambda = 0$, it is immediately apparent in Eq. (33) that, when $k = k_c(V)$, $\Omega[k_c(V);V] = i\omega_c(V)$. The bifurcation is a Hopf one. Equation (33) gives for the quasilength D_{cr} defined in Sec. II B above from the oscillation frequency on the bifurcation line,

$$\frac{\omega_c(V)}{V} = \frac{2\pi}{D_{cr}(V)} = \left\{ \frac{ak_c(V)}{2N_{cr}RTD_0} \right\}^{1/2} . \quad (36)$$

Let us emphasize here that, although our approach yields the same linear bifurcation analysis as Ruina's one, the two models differ in several important respects, even in the low-velocity limit. In the pinning model, inertia is necessarily absent from the "equation of motion" [Eq. (24)] in the creep regime, as a consequence of the creep dynamics itself. The full nonlinear dynamical systems are different and should thus lead, in particular, to different finite amplitude stick-slip dynamics. Indeed, while Ruina's state variable incorporates at once both finite memory and some of the plastic relaxation effects, our age variable only accounts for the memory effect in what we believe to be a more consistent way, plastic relaxation coming into play via the "aging" of the pinning potential. Finally, as will be discussed below, the crossover from creep to inertial motion naturally results from the pinning model, and no externally imposed cutoff on the friction law is needed. We should now compare the above predictions about the SS—steady bifurcation with the experimental results of Sec. II.

a. Position of the SS—steady bifurcation. Let us first concentrate on the experimental results about the bifurcation line $k_c(V)$.

(i) It is immediately apparent in Eq. (34) that $k_c(V)$

should scale with M, as is indeed observed.

(ii) Plugging into Eq. (34) the experimental value [Eq. (6)]

$$-\frac{d[\mu_d(V)]}{d[\ln V]}=b_v=0.014 \; ,$$

we predict for the critical value of k/M (with $D_0=1 \; \mu m$; see Sec. II),

$$(k/M)_c=1.4\times10^5 \; s^{-2} \; ,$$

to be compared with our measured values, which range from 2×10^4 to $1.3\times10^5 \; s^{-2}$. In view of the quite simplistic nature of our model, we consider this as a surprisingly good agreement.

(iii) We now have to face a more difficult question: if we use for $\mu_d(V)$ the fit obtained from our data, we would expect k_c to be V independent, while we measure it to decrease noticeably when V increases, the dependence being quasilinear in $(\ln V)$. If expression (34) is valid, this immediately entails that $\mu_d(V)$ is not strictly linear in $(\ln V)$ but should rather read

$$\mu_d(V)=a_v-b_v\ln(V/V_0)+c_v\{\ln(V/V_0)\}^2 \; ,\qquad(37)$$

with $c_v=-D/2g\{d[(k/M)_c]/d[\ln V]\}$.

From the data displayed in Fig. 2, we get

$$d[(k/M)_c]/d[\ln V]=-1.8\times10^4 \; s^{-2} \; .$$

We can now evaluate the relative variation $\Delta\mu_d/\mu_d$, on the three decades on which μ_d is measured, due to the last term in Eq. (37). We get

$$\Delta\mu_d/\mu_d=4\times10^{-2} \; ,$$

while the global measured variation is of order 3×10^{-1}. This, added to experimental uncertainties on μ_d values, which can be measured only up to an accuracy of a few percent, leads us to conclude that our $\mu_d(V)$ data are compatible with the theoretical prediction.

Conversely, an important physical remark emerges from this discussion. The experimental study of the SS–steady bifurcation appears as a much more powerful tool for obtaining information on friction in the creep regime than the direct study of $\mu_d(V)$, as far as $k_c(V)$ directly measures the variations of μ_d with velocity. Moreover, since k_c is obtained from a study of the dynamics, it can be measured with a much better accuracy.

b. *Oscillation length in the linear creep regime: Dependence on* k, M, V. We have found, by studying the dynamics on the bifurcation line and the relaxation of small perturbations in the steady sliding regime in its vicinity that:

(i) When measured at fixed k and M values, the oscillation length VT_{osc} does not exhibit any systematic variation, on a range of velocities of three decades and within the experimental spread, of order 20% [see Fig. 10(a)]. This must be put in regard to the theoretical prediction [Eq. (33)], from which

$$\frac{2\pi}{VT_{osc}}=\left\{\frac{ak}{2N_{cr}RT}\right\}^{1/2}\left\{1-\frac{aD_0\{k-k_c(V)\}^2}{8N_{cr}RTk}\right\}^{1/2} \; .$$

$$(38)$$

Using expression (36), we find for the predicted variation of VT_{osc}

$$\frac{\Delta(VT_{osc})}{VT_{osc}}\approx\frac{\pi^2}{2}\frac{D_0^2\{k-k_c(V)\}^2}{D_{cr}^2k_c(V)k} \; ,\qquad(39)$$

which we calculate from our data to be at most of order 10%. Again, although experimental limitations do not permit to check Eq. (39) in detail, the measured behavior is compatible with the results deduced from the model.

(ii) Let us now concentrate on the dependence on k and M of the oscillation length in the bifurcation region, which we can define operationally as VT_{osc} as well as D_{cr}, since we have seen that no V dependence of VT_{osc} is measurable. The corresponding results, displayed in Fig. 10(b), show that D_{cr}^2 is well fitted by a linear function of M/k. This result, when compared with the value of this same quantity deduced from Eq. (36) or (38), leads us to conclude that the number of "creeping moles" N_{cr} should scale with M, as could reasonably be expected.

However, one notices that the linear fit in Fig. 10(b) does not extrapolate to zero at large k. Note that we cannot expect our adiabatic approximation to work well in the large-k regime, where total spring elongations become very small (of order of micrometers), i.e., comparable with the expected characteristic scale a of the pinning potential.

c. *An attempt to evaluate the number of contacts.* We are now able to deduce from the slope of the D_{cr}^2 (or VT_{osc}) vs M/k curve the value of N_{cr}/a for a given value of M, here chosen to be 1 kg. We find

$$N_{cr}/a=1.5\times10^{-11} \; mol/\mu m \; .\qquad(40)$$

In order to evaluate a total creeping volume $V_{cr}=N_{cr}v_{mol}$, we have to make a guess about the molar volume v_{mol}. Paper has a very complicated structure (cellulose fibers, glue, loads of various kinds), so that what we have called a mole of creeping degrees of freedom has a very uncertain meaning. So, we will use the most conservative estimate, $v_{mol}\approx20 \; cm^3$, a typical value for small molecules. Then

$$V_{cr}\approx300a$$

with a in micrometers, and V_{cr} in $(\mu m)^3$.

It seems reasonable to think that the surface of an individual contact is of order $D_0^2\sim1 \; \mu m^2$. However, we have no direct information about the effective height h of the active plastic zone. This quantity is certainly strongly dependent on the detailed nature of the plastic processes at play and should therefore be strongly material dependent. An estimate of order $D_0/10$ seems, again, to be a very prudent one.

Finally, we should try to estimate a, which we interpret as the distance traveled, once a contact has been destroyed, until the replacing one is created. A lower limit

corresponds to completely aligned contacts, in which case $a \sim L/n$, where $L = 10$ cm is the lateral extension of our square slider, and n is the total number of contacts.

From this we obtain, with the help of (40), a lower estimate,

$$n = N_{cr} v_{mol} / D_0^2 h \approx 2 \times 10^4 .$$

The pressure on real contacts corresponding to this value is

$$p = Mg / nD_0^2 \approx 5 \times 10^8 \text{ Pa} ,$$

to be compared with typical yield pressures of solids, which range from $\sim 10^8$ to $\sim 10^9$ Pa.

These orders of magnitude appear very satisfactory. However, let us strongly insist that they can at best be considered as indicative of the plausibility of our interpretation.

3. Creeping relaxation: A qualitative interpretation

Let us now consider the experimental situation described in Sec. II B, where the system is rapidly stressed to a level not too far below the static threshold by displacing the free end of the spring to a position x_0 which is then kept fixed. The observed characteristics of the relaxation dynamics can be easily understood qualitatively on the basis of our model: The closer the initial stress to the static threshold, the closer the system to its runaway threshold, i.e., to the depinning condition, so the larger the relaxation amplitude. Contact destruction and renewal occur as a consequence of creep. The age of the contacts decreases as the motion accelerates, which reduces the pinning strength and takes the system closer and closer to runaway; hence the observed self-acceleration.

Equations (29) should be appropriate to describe the very first stage of this motion—still far below threshold. The necessary numerical integration would thus be of limited interest, since it would only provide predictions in the region of very weak amplitudes where precise experimental data are not yet available. Good data correspond to the vicinity of the threshold, where Eyring's results [Eqs. (18) and (19)] are no longer valid. In this region, the dynamics is expected to depend strongly on details of the shape of the pinning potential and of the loss mechanisms, and no detailed general prediction can be formulated. For these reasons we believe that numerical studies on particular models would be premature.

The same kind of qualitative arguments should apply to crept stick near threshold. In this case the stress increase due to continuous pulling provides an added accelerating mechanism. Again, the regime where the dynamics is observed to exhibit scaling properties leading to the characteristic length D_1 corresponds to the vicinity of the depinning threshold. The observation of a scaling itself suggests that this length is related to the characteristic scale of the pinning potential.

4. Crossover and kinetic friction coefficient in the inertial regime

The crossover from what was termed above creep and inertial regimes now appears quite natural in our qualita-

tive picture: it corresponds to the situation where the velocity has become large enough for the driving force piled up on one a traversal to drive the system up to runaway, i.e., into practically free motion. In this situation the system is depinned enough to move quasifreely, i.e., with a velocity of order $(a / \tau_{in}) \approx D_1 / \tau_{in}$, which corresponds to the criterion extracted from experimental data.

In this regime, fluctuation effects are important: the system close to threshold runs away by a series of nonuniformly spaced statistical jumps of one or a few a. We therefore expect the dynamics in the crossover region to be quite noisy. This agrees with the qualitative trend noted in the experiments. Close to threshold, the present single-mode model is certainly insufficient. As is known from the dynamics of extended pinned systems such as charge density waves [26–28] or vortices in type-II superconductors [29], depinning is not a single macroscopic event affecting all elementary units (here, contacts) at once, but in general occurs through avalanche processes. We expect these to occur here as well and to give rise, via internal vibrational couplings between contacts, to a complex spectral signature.

Once the inertial regime has been reached, the initially resting slider is pulled into the depinned state too fast for the creep amplitude to become a noticeable fraction of the spring elongation: stick is almost perfect until runaway is reached, while pinning becomes quasi-irrelevant during slip. When the system is in steady inertial motion, we therefore expect the velocity vs force curve to behave as schematized in Fig. 12: the larger the force, the closer the system approaches the ordinary frictional behavior [Eq. (20)]. That is, due to dissipation into vibrational modes, friction in the depinned state should exhibit velocity strengthening, as is indeed observed.

Our measurements of $\mu_d(V)$ are performed over a limited V range and not very far above threshold. It is seen in Fig. 12 that a linear extrapolation of such data must lead to a finite positive intercept μ_{d0}, in agreement with experiments (see inset of Fig. 4). This analysis therefore suggests that, when the system operates in the inertial regime, its dynamics can quite reasonably be approximated by the standard model of solid friction, that is, (i) stick for forces $F_{ext} < M\mu_s(t_{stick})$; (ii) slip with a velocity-
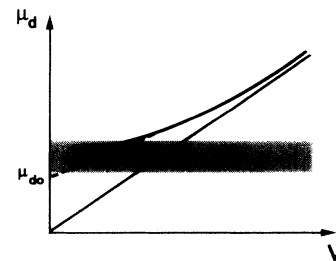

FIG. 12. Schematic representation of $F/Mg = \mu_d(V)$ in the inertial regime. The shaded region corresponds to the regime where such a characteristic loses validity due to slow relaxation effects. The dotted line stands for the linear extrapolation of data measured in a limited velocity range.

strengthening friction coefficient $\mu_d(\dot{x})$ where the μ_d function is the same for steady and unsteady motion, and $\mu_d(\dot{x} \to 0 < \mu_s$.

On the contrary, in the creep-dominated part of parameter space, the standard model is not acceptable. The dynamics is controlled by Brownian motion in an age (i.e., dynamical history) -dependent pinning potential. Stick is no longer perfect. Moreover, it is no longer possible to extrapolate from the steady $\mu_d(V)$ a unique $\mu_d(\dot{x})$.

IV. CONCLUSION

We believe that the study presented here provides, when compared with previous results on rocks and metals, strong support to the —a priori rather surprising— idea that low-velocity friction dynamics obeys quite general laws whose functional form is material independent. The number of relevant control parameters—loading mass, machine stiffness, pulling velocity—is small enough for extensive study of a given system to be feasible. Experimental results can be rationalized on the basis of a model that, although simplistic, seems to provide an acceptable basic framework. In particular, experimental results on the SS–steady bifurcation are in very satisfactory quantitative agreement with theoretical predictions. In particular, not only does this analysis show our heuristic description to be consistent with the data, but it leads us to a physical statement; namely, we conclude that the amount of matter actually involved in the creep process scales with the slider mass. Moreover, our numerical estimates seem consistent with the fact, suggested by the works of Bowden and Tabor and by Rabinowicz, that the plastic processes at work in low-velocity friction occur within effective contact volumes of submicrometer size.

The nature of the system appears in the model only via a few material-dependent parameters that we associate, following previous authors, with surface roughness, plastic relaxation dynamics, and average contact size. Our interpretation in terms of thermal creep in an aging pinning potential leads us to correlate the suspected universality of low-velocity dynamics with the fact that activated processes are quite insensitive to details of the potentials in which they take place.

This work obviously calls for a number of confirmations and extensions in various directions:

(i) Further quantitative investigations of our paper-on-paper system. In particular, as already mentioned, detailed noise studies should be of interest.

(ii) Extensive studies on different classes of solids, in particular metals with known bulk microscopic structures and plastic properties. We have performed a few preliminary experiments on duralumin-duralumin, which give evidence of the existence of the creep regime.

If universality of the creep dynamics is confirmed, theoretical developments will be necessary, along two main directions. On the one hand, numerical studies based on the single-mode model proposed here, or on an improved version allowing for random pinning will then become worth performing. On the other hand, we will have to try to correlate the present model with a more detailed description of the contacts and of their statistics, possibly in the spirit of the recent work of Bréchet et al. [30] and of Jensen, Bréchet, and Doucot [31]. It will certainly then appear, as is the case for charge density wave transport and vortex dissipation, that a one-mode approximation is too crude to account for more detailed features of the dynamics.

(iii) Behavior of systems of much lower internal stiffness. We can then hope to reach regimes where internal spatial couplings become relevant and may give rise to the kind of extended system behavior studied by recent earthquake models [7,18,19].

[1] F. P. Bowden and D. Tabor, Friction and Lubrication of Solids (Clarendon, Oxford, 1950).

[2] E. Rabinowicz, Friction and Wear of Materials (Wiley, New York, 1965).

[3] C. H. Scholz, The Mechanics of Earthquakes and Faulting (Cambridge University, Cambridge, England, 1990), Chap. 2, and references therein.

[4] J. N. Israelachvili, Surf. Sci. Rep. 14, 109 (1992).

[5] S. Granick, Mater. Res. Soc. Bull. 16, 33 (1991), and references therein.

[6] P. A. Thompson and M. O. Robbins, Science 250, 792 (1990); Phys. Rev. A 41, 6830 (1990).

[7] J. M. Carlson and J. S. Langer, Phys. Rev. A 40, 6470 (1989).

[8] Y. Gu and T. F. Wong, in Rock Mechanics, Proceedings of the 33rd U.S. Symposium, edited by J. R. Tillerson and W.

R. Wawersik (Balkema, Rotterdam, 1992); in Non-Linear Dynamics and Predictability of Critical Geophysical Phenomena, edited by A. Gabrielov and W. Newman, AGU Physical Monograph No. 83 (AGU, Washington, DC, 1994).

[9] J. T. Oden and J. A. C. Martins, Comput. Methods Appl. Mech. Eng. 52, 527 (1985).

[10] A. Ruina, J. Geophys. Res. 88, 10 359 (1983).

[11] J. R. Rice and A. L. Ruina, J. Appl. Mech. 50, 343 (1983).

[12] E. Rabinowicz, Proc. Phys. Soc. London 71, 668 (1958), and references therein.

[13] J. T. Burwell and E. Rabinowicz, J. Appl. Phys. 24, 136 (1953).

[14] J. H. Dieterich, J. Geophys. Res. 84, 2161 (1979).

[15] J. H. Dieterich, Pure Appl. Geophys. 116, 790 (1978).

[16] Reference [3], p. 78.

[17] J. C. Gu, J. R. Rice, A. L. Ruina, and S. T. Tse, J. Mech. Phys. Sol. **32**, 167 (1984).

[18] R. Burridge and L. Knopoff, Bull. Seismol. Soc. Am. **57**, 341 (1967).

[19] J. R. Rice, J. Geophys. Res. **98**, B6, 9885 (1993).

[20] "Contre-collé Bristol" Ref. D2B No. 274520, manufactured by Papeteries Canson et Montgolfier SA, France, a subsidiary of Arjo-Wiggins-Appleton, USA.

[21] "Electro-Mike Control," manufactured by Electro Corporation, Sarasota, FL.

[22] H. Eyring, J. Chem. Phys. **4**, 283 (1936).

[23] K. Glasstone, J. Laidler, and H. Eyring, *The Theory of Rate Processes* (McGraw-Hill, New York, 1941).

[24] See, for example, C. W. Gardiner, in *Handbook of Stochastic Methods*, edited by H. Haken, Springer Series in Synergetics Vol. 13 (Springer-Verlag, Berlin, 1990).

[25] P. Nozières (unpublished).

[26] G. Gruner, Physica D **8**, 1 (1983).

[27] P. A. Lee and T. M. Rice, Phys. Rev. B **19**, 3970 (1979).

[28] D. S. Fisher, Phys. Rev. B **31**, 1396 (1985).

[29] A. I. Larkin and Yu. N. Ovchinnikov, J. Low Temp. Phys. **34**, 409 (1979).

[30] Y. Bréchet, B. Doucot, H. J. Jensen, and A. C. Shi, Phys. Rev. B **42**, 2116 (1990).

[31] H. J. Jensen, Y. Bréchet, and B. Doucot, J. Phys. I **3**, 611 (1993).

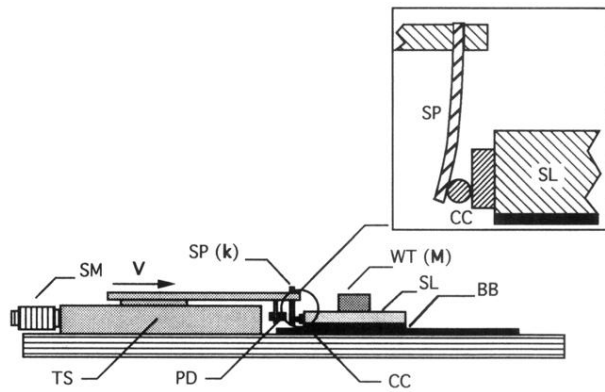FIG. 1. Low-velocity friction setup $(10^{-2} \ \mu\text{m s}^{-1} < V < 10^3 \mu\text{m s}^{-1})$. BB, Bristol board; CC, crossed cylinders contact; PD, position detector; (SL, slider; TS, translation stage; SM, stepping motor; SP, cantilever spring of stiffness k; WT, calibrated weights. The mass of SL plus WT is M. In the high-velocity version $(10^2 \ \mu\text{m s}^{-1} < V < 5 \times 10^4 \ \mu\text{m s}^{-1})$, the brass cantilever spring (SP) is replaced by a helicoidal steel spring. The inset shows a magnified detail of the crossed cylinders contact between the bent cantilever spring (SP) and the slider (SL).
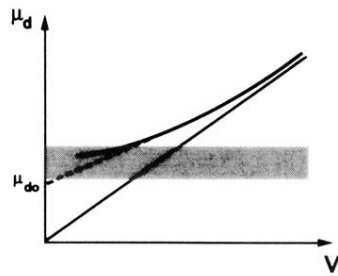
FIG. 12. Schematic representation of $F/Mg = \mu_d(V)$ in the inertial regime. The shaded region corresponds to the regime where such a characteristic loses validity due to slow relaxation effects. The dotted line stands for the linear extrapolation of data measured in a limited velocity range.